Research Square

Preprints are preliminary reports that have not undergone peer review.
They should not be considered conclusive, used to inform clinical practice,
or referenced by the media as validated information.

Vegetation-based Approach for Rotational Landslide Activity Classification: Case Study of Kundasang, Sabah

Mohd Radhie Mohd Salleh (mohdradhie.gis@gmail.com)
Universiti Teknologi Malaysia
Muhammad Zulkarnain Abdul Rahman
Universiti Teknologi Malaysia
Zamri Ismail
Universiti Teknologi Malaysia
Mohd Faisal Abdul Khanan
Universiti Teknologi Malaysia
Kasturi Devi Kanniah
Universiti Teknologi Malaysia
Azman Ariffin
Universiti Teknologi Malaysia
Wan Hazli Wan Kadir
Universiti Teknologi Malaysia
Tze Huey Tam
Universiti Teknologi Malaysia
Mohd Asraff Asmadi
Universiti Teknologi Malaysia

Research Article

Keywords: Landslide, GIS, Remote Sensing, Machine Learning, Vegetation

Posted Date: May 30th, 2023

DOI: https://doi.org/10.21203/rs.3.rs-2982134/v1

License: This work is licensed under a Creative Commons Attribution 4.0 International License.
Read Full License

Additional Declarations: No competing interests reported.

Vegetation-based Approach for Rotational Landslide Activity Classification: Case Study of Kundasang, Sabah

Mohd Radhie Mohd Salleh, Muhammad Zulkarnain Abdul Rahman, Zamri Ismail, Mohd Faisal Abdul Khanan, Kasturi Devi Kanniah, Azman Ariffin, Wan Hazli Wan Kadir, Tam Tze Huey, and Mohd Asraff Asmadi

Abstract

Background: Mapping and monitoring the state of activity of landslides is crucial for effective landslide management and risk assessment. This study presents a novel approach using vegetation anomalies indicator (VAI) derived from high-resolution remotely sensed data for landslide state of activity mapping. The study focuses on the Kundasang area in Sabah, Malaysia, known for its tectonic activity. High-resolution remotely sensed data were utilized to assist in the manual inventory process of landslide activities and to generate VAIs as input for modeling.

Results: The landslide inventory process identified active, dormant, and relict landslides. The resulting inventory map was divided into training (70%) and validation (30%) datasets for modeling purposes. Seven main VAIs, including canopy gap, mature woody vegetation, primary forest, Root Strength Index (RSI), and water-loving tree, were produced and used as the input for the classification process using Support Vector Machine (SVM) and Artificial Neural Network (ANN) methods. The result showed that SVM outperforms ANN for both deep-seated and shallow rotational landslides, with an overall accuracy of 68.6% and 80.7%, respectively. Furthermore, an evaluation of SVM revealed that the radial basis function (RBF) kernel yielded the highest accuracies, whereas ANN performed best with a hyperbolic tangent (*tanh*) activation function.

Conclusion: The accurate classification of landslide state of activity using VAI provides several benefits, including the ability to map and classify landslide activity in forested areas, characterize vegetation characteristics specific to each activity state, and enable continuous monitoring in areas where field monitoring is impractical. This research opens new possibilities for more accurate landslide activity mapping and monitoring, thereby improving disaster risk reduction and management in tectonically active regions.

Keywords Landslide, GIS, Remote Sensing, Machine Learning, Vegetation

Introduction

Detailed landslide inventories and landslide information are crucial in landslide studies. Landslide inventory maps have been produced for various reasons (Brabb, 1991): (i) documenting landslide phenomena in different areas, from small to large watersheds (Cardinali et al., 2001), (ii) documenting landslide occurrences at regional, state, and national levels (Brabb and Pampeyan, 1972, Cardinali et al., 1990, Duman et al., 2005), (iii) as a precursor to producing landslide susceptibility, hazard and risk assessment (Van Westen et al., 2006, Hung et al., 2017) and (iv) analyzing the landslide distribution, types and patterns related to drainage, terrain morphological and, vegetation characteristics (Guzzetti et al., 1996, Soeters and Westen, 1996). However, information on the state of activity is still not up-to-date (Kalia, 2018) and is hampered by several conditions. It is a major challenge to detect and map the landslides present and assess the state of activity for several reasons, for instance, the high dense tree canopy covering (Jaboyedoff et al., 2012, Van Den Eeckhaut et al., 2013, Pirasteh and Li, 2016, Mezaal et al., 2017b, Salleh et al., 2018), the undulating area (Brardinoni et al., 2003, McKean and Roering, 2004, Korup, 2005, Cigna et al., 2013, Tien Bui et al., 2018), and the rapid vegetation growth (Brardinoni et al., 2003, Musinguzi and Asiimwe, 2014, Pradhan et al., 2015, Mezaal et al., 2017b, Mezaal et al., 2017a, Samodra et al., 2017, Samodra et al., 2018). These factors remove the landslide signature and complicate the determination of a landslide boundary and state of activity.

Previously, landslide inventory mapping involved the practice of field mapping. An interpreter can recognize landslide types and activities based on several diagnostic features. For instance, active slides are commonly fresh; that is, their terrain morphological features, such as scarps and ridges, are easily recognizable as being due to gravitational movement, and they have not been significantly modified by the surficial processes of weathering and erosion (Varnes, 1978). However, due to the vast extent of the observed areas and access difficulties, this type of slope instability investigation is not always economically or practically feasible for conducting a systematic investigation of landslide phenomena at the regional scale, in which time-consuming and resource-intensive procedures are required (Guzzetti et al., 1999, Haneberg et al., 2009, Santangelo et al., 2010, Cigna et al., 2013, Behling et al., 2014, Pawłuszek et al., 2017, Yang et al., 2017, Perera et al., 2022). This procedure also is hampered by several challenges, especially old landslides, which make it impossible to see all the parts of a landslide; total or partial vegetation coverage; and features dismantled by other landslides or human actions, such as agricultural work (Guzzetti et al., 2012).

Due to the wide area coverage, non-invasive nature, and cost-effectiveness of remotely sensed data, integrating and complementing conventional investigations with remote sensing techniques represents a valuable source of support for landslide mapping (Moosavi et al., 2014, Golovko et al., 2015, Bozzano et al., 2017). As stated by Scaioni et al. (2014), remote sensing has been utilized in three primary areas of landslide applications, namely landslide recognition, landslide monitoring, and landslide susceptibility and hazard assessment. The landslide monitoring involves closely observing the changes in the state of activity of a landslide over time, as it undergoes a failure process. Majority of the studies monitor the activity of landslides by using quantitative measurements of ground deformation, surface point displacements (also known as deformation measurement), changes in geotechnical or geophysical parameters, and water table level measurements. Remote sensing techniques are used to measure changes on the surface of slopes, which are important indicators for understanding landslide development and identifying correlations with triggering factors. The interpretation of aerial photographs, considered the most common technique used in landslide recognition (Otukei and Blaschke, 2010, Guzzetti et al., 2012, Chen et al., 2013, Li et al., 2016), is also capable of covering a wide area. However, this technique requires experience, training, and a well-defined landslide interpretation standard (Antonini et al., 2002, Galli et al., 2008, Jackson Jr et al., 2012). Furthermore, the technique may also produce some mapping errors (Marchesini et al., 2013, Santangelo et al., 2015), especially for forest areas (Brardinoni et al., 2003, Mezaal et al., 2017a, Pirasteh and Li, 2016), since the reflectance spectra of vegetation conceal the spectra of underlying soils and rocks, the most critical barrier to geological identification and mapping (McKean and Roering, 2004, Hede et al., 2015). In addition, the use of monoscopic and stereoscopic images from aerial photographs might produce a digital terrain model (DTM) with low accuracy since the ground surface is not well presented in photogrammetric DTMs of forested terrain, which leads to incomplete and unreliable landslide inventories.

Furthermore, to precisely compare corresponding areas and measure deformations, it is necessary to have a series of repeated images that are accurately registered. Other remote sensing technologies, such as synthetic aperture radar (SAR) sensors, primarily measure surface deformations and construct time series of surface deformations at single points (Berardino et al., 2002, Hooper et al., 2007, Cigna et al., 2011, Jaboyedoff et al., 2012, Bianchini et al., 2017). Bozzano et al. (2017) used Persistent Scatterer Interferometry (PSI) to compute time series surface deformation from satellite data captured in space which enabled the determination of both the vertical and horizontal (east-west) components of the movement. However, this method uses an active sensor and the data acquisition depends on various factors such as the natural illumination, foreshortening, layover effects, atmosphere propagation effects, and vegetation decorrelation in forested terrain. High temporal resolution datasets are also required.

Recently, new methods and technologies have been exploited by researchers to detect and map landslides (Guzzetti et al., 2012). One of these technologies is airborne LiDAR (Light Detection and Ranging). The ability of high-density airborne LiDAR data to penetrate vegetation and provide the topographic surface is critical to detecting and mapping landslides under forested areas (Haugerud et al., 2003, Van Den Eeckhaut et al., 2007, Pirasteh and Li, 2016, Bibi et al., 2017). LiDAR derivative products such as contour maps, shaded relief, slope, and curvature can be used in further landslide detection and mapping (Guzzetti et al., 2012, Jaboyedoff et al., 2012, Bibi et al., 2017). Nevertheless, the main limitations of this technique are the cost of data acquisition (Joyce et al., 2014, Gaidzik et al., 2017, Luo et al., 2018) and the time-consuming data processing, especially for large areas. The combination of airborne LiDAR and terrestrial LiDAR (TLS) can greatly assist in investigating landslide activity. However, in forested areas with complex topography and uneven terrain, limited line-of-sight access can pose challenges for terrestrial LiDAR data collection. Obstacles such as trees, shrubs, and understory vegetation can hinder the positioning of LiDAR scanners and limit the coverage of the target area, potentially resulting in incomplete and non-representative data. This limitation can affect the accuracy and reliability of landslide analysis, as the data may not fully capture the extent and characteristics of landslides in forested areas. It is important to consider and address these challenges when utilizing terrestrial LiDAR in forested landslide-prone regions for comprehensive and accurate landslide studies. As a result, most studies have generally covered a small area (less than 20 km2) (Guzzetti et al., 2012). The technique also requires experience, training, and a well-defined standard for LiDAR data processing and landslide interpretation. Even though of high-density airborne LiDAR data could penetrate the vegetation and provide the topographic surface, the tree canopy can scatter or absorb the LiDAR beams, resulting in incomplete or obscured data, especially in areas with dense foliage or tall trees. LiDAR signals may not penetrate the forest canopy to reach the ground surface, in resulting limited ground point, leading to incomplete or inaccurate data. This can make it challenging to accurately map landslides that occur beneath the forest canopy, especially if the forest is dense or has multiple canopy layers.

Besides that, geomatics techniques are also widely used for landslide state of activity analysis (Artese and Perrelli, 2018). In a tropical vegetated area, landslide analysis requires frequent site visits, real-time deformation monitoring, and expensive instruments such as electronic distance meters (EDM), which are installed in the landslide area for monitoring purposes (Stiros et al., 2004, Tsai et al., 2012, Afeni and Cawood, 2013, Castagnetti et al., 2013, Corsini et al., 2013, Simeoni et al., 2015). However, this method involves some obstacles, especially in active landslide zones where enormous financial outlays may be lost and instruments incur costly damage once the landslide strikes.

For all these reasons, the application of vegetation as an indicator of landslide state of activity may be an effective, natural, and inexpensive approach for landslide inventory and monitoring processes, especially in tropical regions. Apart from using surface terrain information to identify landslide activity, the inclusion of information regarding surface objects, such as vegetation, yields noteworthy insights into landslide sate of activity. As silent witnesses, trees may be displaced, tilted, partially buried, bent, or limited in growth by landslides. Vegetation may have a beneficial impact on the stability of a slope because the roots reinforce the layers by binding the soil. To determine the relationship between vegetation characteristics and landslide occurrences, several VAIs have been used, such as tree height irregularities, leaning trunk, and tree-ring. Razak et al. (2013) found that trees in active landslide areas are characterized by low vegetation, small crowns, and irregular tree height. Tree trunks are often curved as a result of external factors including catastrophic events, the unavailability of light, and soil creep (Zhang et al., 2016). If trees frequently grow with curved trunks on slopes where other evidence indicates the occurrence of creep, this strongly suggests that their curvature is due to creep (geotropism) (Harker, 1996). Wang et al. (2016a) and Wang et al. (2016b) also demonstrated the application of TLS in characterizing tree stem curves. They found that most trees inside landslide (shallow) areas had curved stems due to the effects of soil movement. The utilization of dendrochronological or tree-ring analysis methods could enhance the understanding of landslide state of activity and risk (Łuszczyńska et al., 2017) since stem deformations affect the structure of wood and tree-rings (Stefanini, 2004, Wistuba et al., 2013). However, using tree rings to study landslide behavior has certain limitations; for example, some trees need to be felled, which is impossible in places such as forest nature reserves. Many academic investigations also explore the impact of diverse vegetation indices, such as the Normalized Difference Vegetation Index (NDVI), as a means of assessing and monitoring the state of landslide activity (Zhong et al., 2021, Xun et al., 2022, Satriano et al., 2023). Overall, the existing studies have focused on single landslide types and activity, while a limited number of indicators were used. No library has yet been produced by compiling all the related vegetation indicators of landslides for different landslide scenarios. Therefore, this study aims to employ vegetation anomalies as an indicator for landslide state of activity classification using multi-resolution remotely sensed data.

Materials and Methods

Study Area

Kundasang is located in the northwest of Ranau, Sabah (Figure 1) and generally well known for its unstable hilly area. The study area covers 70.47 km^2 and is situated between 500 and 2000 m above mean sea level. The hilly terrain and ridges, with their high elevation and combinations of steep slopes, are the consequence of violent historical tectonic activity (Tating, 2006). The climate of the study area is determined by its proximity to the equator; it is humid and tropical, with temperatures ranging between 25 °C and 35 °C in lowland areas. This area has two monsoon seasons: the "dry" monsoon from May to October and the "wet" monsoon from November to April. Since Kundasang is within an area known as the “ever-wet zone”, it receives at least 60 mm of rainfall per month, while the annual rainfall ranges from 1920 mm to 3190 mm (average 2075 mm) (Tating et al., 2013). The choice of this area as the location in which to pursue the study objective was because of its tropical environment and abundant landslides caused by natural and anthropogenic factors.

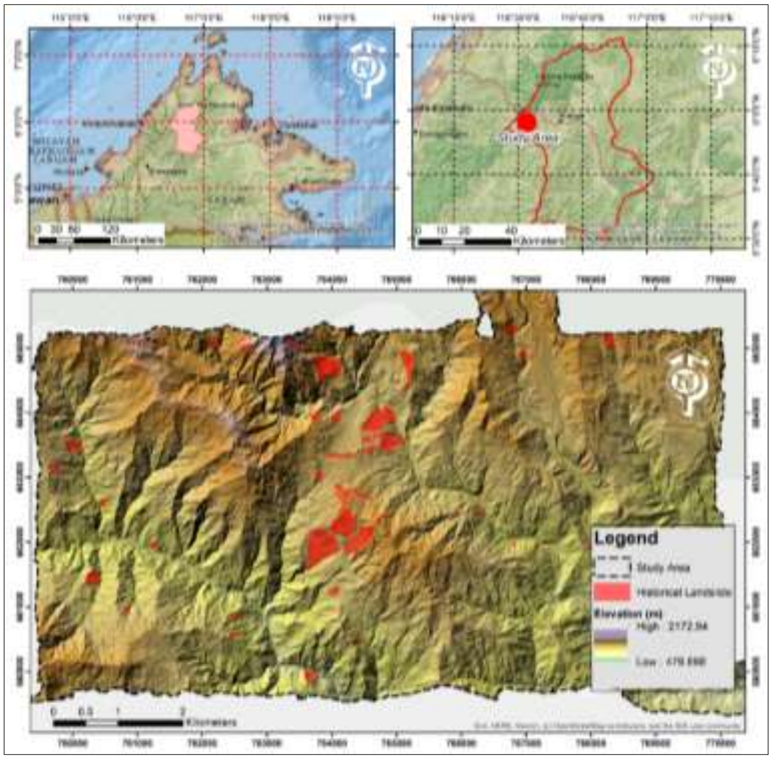

Figure 1. Location of study area

Geologically, the Kundasang area consists of several types of lithology, such as the Crocker Formation (Late Eocene to Early Miocene age) and the Trusmadi Formation (Paleocene to Eocene age), granite intrusion, and several recent Quaternary alluvial materials which are still being deposited (Tongkul, 1987, Roslee et al., 2008). The Trusmadi Formation, in general, exhibits two distinct structural orientations - NW-SE and NE-SW (Tongkul, 2007, Roslee et al., 2020).- and is characterized by the presence of dark-colored argillaceous rocks, siltstone, and thin-bedded turbidite in a well-stratified sequence (Yusoff et al., 2016, Roslee et al., 2020). Jacobson (1970) divided the Trusmadi Formation into four main lithological units: argillaceous rocks, interbedded sequences (turbidites), cataclasites, and massive sandstones. The Crocker formation in the study area is composed of inter-bedded shale and sandstone (Azlan et al., 2016) with four lithology units, namely thick-bedded sandstone, thinly bedded sandstone and siltstone, red and dark shale, and slumped deposits (Jacobson, 1970). Due to the extensive deformation and discontinuity in the arenaceous Crocker Formation's sandstone and shale beds, they are prone to weathering and instability.

Methodology

Overall, this study consists of several phases. The first phase concentrates on the data acquisition and pre-processing of high resolution remotely sensed data, field data and ancillary data collection. The remotely sensed data, i.e., airborne LiDAR, aerial photos and high-resolution satellite images were georeferenced into the same coordinate system. The point clouds obtained from the airborne LiDAR data were filtered to remove the non-ground points. The ground points were interpolated to produce Digital Terrain Model (DTM). Digital Surface Model (DSM) was produced by interpolating the non-ground points. The normalized point clouds were generated by normalizing the original point clouds based on DTM.

The field data collection including landslide inventory and vegetation characteristics. The second stage focused on the development of landslide inventory using manual interpretation of high resolution remotely sensed data. The landslide inventory map was validated using field-based landslide inventory data. The third stage emphasized on the development of VAIs using high resolution remote sensing data. The VAIs consisted of 15 raster maps that can be grouped into 7 groups: 1) tree height irregularities; 2) canopy gap; 3) density of different layer of vegetation; 4) vegetation type; 5) vegetation indices; 6) root strength index (RSI); and 7) distribution of water-loving trees. All the VAI maps and landslide inventory maps obtained from the manual interpretation were used in the fifth stage that aimed at classifying landslide activities based on machine learning-based approaches. Finally, the classified landslide activity map was evaluated using the landslide inventory map.

Landslide Inventory

Landslide inventory was produced based on the combination of remote sensing data interpretation and field observation. The remote sensing-based landslide inventory was done using several airborne LiDAR-derived datasets, i.e., topographic openness, hillshade, and color composite. These datasets were generated using DTM and orthophoto with 7 cm spatial resolution. Topographic openness was used to observe the clear contrast between the planar surface and down-slope surface (Razak, 2014). It can be one of the landslide features that can be recognized through color ramp observations. The hummocky surface of the hillshade, steep slope of the hillshade 3D features (Razak, 2014, Soeters and Westen, 1996, Crawford, 2014), thick toe structure of the landslide area, and step-like morphology on the hillshade image (Van Westen and Getahun, 2003) can be used to recognize the landslide body. Orthophoto image is capable of exhibiting any evidence of landslide occurrence either in a clear form of landslide polygon or other evidence leading to landslides, for example road crack, soil erosion, and bad surface or ponding in niches or back tilting area (Van Westen and Getahun, 2003).

Next, the inventory process continued with landslide delineation. The delineation process was conducted based on a scarp and accumulation area where the scarp area covered from the crown part until the head, while the accumulation area covered from the main body until toe. For assigning the landslide type and activity several signatures were observed which related to morphology, vegetation, and drainage characteristics. For active landslides, the scarp and crown are obvious, and the accumulation zone is visible. The area is mostly characterized by less or almost no vegetation cover. A dormant landslide is an inactive landslide that may be reactivated due to its original causes or other causes. The scarp and body of the failure are still visible in the LiDAR dataset with low density vegetation and does not show any recent activity. A relict landslide is an inactive landslide, where the slope has been stabilized due to natural factors or mitigation measures. The scarp and body of the landslide area are not distinguishable through LiDAR dataset. Meanwhile the area is densely covered by vegetation or has been mitigated by any structural measures. The results of remote sensing-based landslide inventory were verified and corrected using the field-based inventory.

Parameterization of vegetation anomalies using remotely sensed data

In this study, seven groups of VAIs were used in landslide activity classification i.e., tree height irregularities, canopy gap, different layers of vegetation, vegetation type distribution, vegetation indices, root strength index, and distribution of water-loving trees. All the VAIs were derived from airborne LiDAR and high-resolution satellite images.

Tree Height Irregularities

Tree height is defined as the perpendicular distance between the top and base of a tree (Verma et al., 2016). The height value varies across different stands and/or species (Rupšys, 2016). The distribution of the tree height significantly reflects the quality and quantity of tree stand and its future growth. Trees in landslide areas have relatively low height, small crown, and more irregularities (Razak et al., 2013, Rupšys, 2016, Mohd Salleh et al., 2019). The tree height irregularities were calculated from the LiDAR-derived CHM. The capability of airborne LiDAR technology to provide high-resolution ground and surface information in gentle surface areas, extensive coverage, and fast data acquisition, makes it an efficient tool for generating this VAI. Tree height irregularities were calculated using the standard deviation of tree height within a 5 m kernel size. A high standard deviation indicates highly irregular tree heights in a specific area, while a low standard deviation indicates that the area is close to the mean (low irregularity).

Canopy Gap

The canopy gap is a "hole" in the forest canopy cover down to a specified height (for example, 2 m) above the ground (Brokaw, 1982). Muscolo et al. (2014) identified the canopy gap as empty areas within forest canopies caused by natural disturbances and which can be filled by other trees (Watt, 1947, Whitmore, 1982). A strong relationship has been found between landslides and forest canopy gaps (Zirlewagen and von Wilpert, 2001, Moos, 2014, Wu et al., 2016). The presence of landslides under a forested area is believed to be detectable by measuring the gaps in the area (Moos, 2014). The production of a tree canopy gap involves several important steps, including the separation of forested areas from non-forested areas, individual tree crown delineation, and tree canopy gap generation. The separation of the forested and non-forested areas was performed by semi-automated identification from the Pleiades images using the SVM image classification method in ENVI software, followed by manual corrections via visual interpretation. The delineation of individual tree crowns was ascertained from the CHM dataset within the forested area using the inverse watershed segmentation method (Rahman and Gorte, 2009). Next, the segmented tree canopy (over 3 m in height) was converted into grid format and the tree canopy gap density was calculated within a 10 m grid. An area with a low number of canopy pixels was considered to have a high canopy gap density.

Density of Different Layers of Vegetation

The density of different vegetation layers was measured using the overall relative point density (ORD) method (Ismail et al., 2015, Campbell et al., 2018). This is intended to compute the density of point clouds for each height class within a specific grid size (5 m grid was used in this study). The layer of vegetation was divided based on the tree height classification schema outlined by Ginzler et al. (2005) i.e., low vegetation, young woody vegetation, matured woody vegetation, and old forest. To calculate the point cloud density, the point count operation was performed. This returned the number of point clouds of a given pixel size. This operation was conducted for both the extracted point clouds and the raw non-ground point clouds. The vegetation layer density was calculated by dividing the raster layers of individual vegetation classes based on the height value and the raw non-ground pixels, then converting every pixel into a percentage unit.

Vegetation Type Distribution

According to Malaysian Standard 1759 (MS 1759:2004), many categories of vegetation type can be classified. In the current study, four vegetation types were used, such as grass, secondary forest, primary forest, and agriculture. Landslide occurrence was higher in logging areas, secondary forest and settlement areas, and lower in primary forest areas (Pradhan, 2013, Shahabi and Hashim, 2015). This indicator was mapped from satellite imagery and LiDAR-CHM datasets.

Vegetation Indices

Vegetation indices are mathematical transformations designed to assess the spectral contribution of vegetation to multispectral observations. The bands normally used are Green, Red, and Near Infrared (NIR). These vegetation indices operate by contrasting intense chlorophyll pigment absorptions in the red band against the high reflectivity of plant materials in the NIR. As one landslide area criterion is the low presence of vegetation, it was essential to analyze anomalies using this dataset. The six vegetation indices were derived from Pleiades imagery as described below:

$$NDVI = \frac{(NIR - R)}{(NIR + R)} \tag{1}$$

$$DVI = NIR - R \tag{2}$$

$$SAVI - \frac{(NIR - R)}{(NIR + R + L)} X (1 + L) \tag{3}$$

$$OSAVI = \frac{(NIR - R)}{(NIR + R + L)} X (1 + 0.16) \tag{4}$$

$$GDVI = NIR - G \tag{5}$$

$$GNDVI = \frac{(NIR - G)}{(NIR + G)} \tag{6}$$

where *NIR* is the near-infrared band, *R* is the red band, *G* is the green band, and *L* is the correction factor.

Root Strength Index (RSI)

Root strength is a soil reinforcement factor (Abdi, 2018). Increasing its strength will further reinforce the soil (Stokes, 2002). Changing the tree root strength affects slope stability (Schmidt et al., 2001, Iwahashi et al., 2014, Capilleri et al., 2016). The root strength index (RSI) was derived from the estimated tree height and tree density (Iwahashi et al., 2014). The process begins with individual tree crown delineation using the CHM dataset and the estimated tree height was obtained from the airborne LiDAR data, while tree density was defined as the number of trees in a 30 m grid. Equation 8 shows the product of the tree height and the square root of the estimated tree density, which are used to calculate RSI values.

$$RSI = H\ X\ \sqrt{D} \qquad (7)$$

where H is the tree height, and D is the estimated tree density.

Water Loving Trees

Water-loving trees, also known as hydrophytes, are usually found in all forms of wetlands, either in or on the water, or where soils have been flooded or saturated long enough for anaerobic conditions to have been established in the root zone (Cronk and Fennessy, 2016). The distribution of water-loving trees indicates the high presence of active landslides (Chatwin and Howes, 1991, Johnson et al., 2000). In this study, the distribution of water-loving trees was produced by combining aerial photographs, satellite imagery, CHM, and the topographic wetness index (TWI) datasets. Water-loving trees were characterized by their lower height value, i.e., 1 to 3 meters (Chatwin and Howes, 1991). The vegetated pixel area was classified automatically from the satellite imagery. The height values of the vegetation pixels were extracted from the CHM dataset and a pixel value of one to three meters was used for the estimation of water-loving trees. The presence of low vegetation and high TWI values for a certain area indicates a high density of water-loving trees.

Machine Learning for Landslide Activity Classification

Support Vector Machine (SVM)

The SVM was initially developed to find a hyperplane that would optimally separate two classes (i.e., landslides with a specific activity and other landslide activities) (Vapnik, 2013) by maximizing the class boundary margins for linearly separable cases (Abe, 2005). The optimum hyperplane was derived from support vectors with values closest to the classification margin (Gove and Faytong, 2012, Kavzoglu et al., 2014). New data can be classified once the decision surface has been acquired (Tien Bui et al., 2012, Pradhan, 2013, Razavian et al., 2019). This study used a training set of instance-label pairs (xi, yi), i = 1,…,m, where xi ∈ Rn and yi ∈ (1,-1), xi are an input space vector that represents all the VAIs, such as the tree height irregularities, canopy gap, and vegetation indices. Meanwhile, (1,-1) represents the landslide and non-landslide pixels, which were categorized into different states of activities (i.e., active, dormant, and relict). However, classification with linear functions is highly challenging. In this case, a non-linear approach could be performed using kernel functions (i.e., polynomial, radial basis function, and sigmoid) (Ian H. Witten, 2017, Kotu and Deshpande, 2014, Ayalew and Yamagishi, 2005).

In the SVM modeling approach, several parameters needed to be configured, such as the kernel function, regularization parameter (C), gamma (γ), and degree of the polynomial (d). These parameters are crucial to finding a model that performs a good classification task (Silva and Eugenio Naranjo, 2020). Parameter C can monitor any overfitting activity of the model, while parameter γ controls the model's degree of non-linearity. In this study, three SVM kernel functions were used: Linear (SVMl), Polynomial (SVMP), and RBF (SVMR). The selection of parameter values of C, γ, and d were finalized by applying the Grid Search (GS-SVM) and Genetic Algorithm (GA-SVM) optimization techniques.

The GS-SVM technique comprises an in-depth search of a particular parameter interval. It functions by assessing the performance and evaluation of the sample data for a specific parameter value. This can be accomplished by first generating a range of C and γ values, as well as a d value, for the polynomial kernel to search through. The cross-validation (CV) technique with 10-fold was used as a performance metric, aiming to identify the optimum hyper-parameter combination that would enable the classifier to accurately predict unknown data. Genetic algorithm (GA) are stochastic search algorithms inspired by the basic principles of biological evolution and natural selection. GA simulates the evolution of living organisms, in which the fittest individuals come to dominate the weaker ones, by mimicking the biological mechanisms of evolution, such as selection, crossover, and mutation.

Artificial Neural Network

In this study, the ANN method with a Multi-Layer Perceptron (MLP) was used for the landslide activity classification since this algorithm has been the most frequently used in landslide studies. The MLP is a widely used artificial neural network model and can model highly non-linear data with high complexity (Haykin, 2004). MLP models consist of several components and start when the relevant input parameters are fed into the network. These input parameters generate input signals, which are transmitted throughout the network to the hidden layer and the output layer. The scaled input vector, which is introduced by neurons in the input layer, is multiplied with weights, which is a quantity that represents a real number. The neuron in the hidden layer accumulates all this information, including bias.

To classify landslide activity accurately, supervised learning is used to ensure that the desired output is learned. Numerous training algorithms are available for fitting the model to the intended output. In this study, five types of learning algorithms were used, namely backpropagation (*backprop*), resilient backpropagation with weight backtracking (*rprop+*), resilient back propagation without weight backtracking (*rprop-*), a globally convergent algorithm with the smallest absolute gradient (*sag*), and a globally convergent algorithm with smallest learning rate (*slr*). The role of the activation or transfer function in a neural network is to produce a non-linear decision boundary via non-linear combinations of the weighted inputs. This transforms a set of input signals into an output signal. This transfer function introduces non-linearity into the MLP model, distinguishing it from the linear model. This study used two activation functions that are widely used in MLPs: sigmoid (*logistic*) and hyperbolic tangent (*tanh*). To train the optimum MLP network configuration, the learning rate was set to 0.01. This helped to prevent the network from diverging from the target output and improved the general performance.

Therefore, considering the MLP topology and criteria stated above, several networks consisting of a three-layered MLP were trained to optimize or find the best activation function of the hidden and output layers, as well as the number of nodes or neurons in the hidden layer.

Results Validation

To track the progress of individual landslides, an error matrix reflecting the sample segments assigned to a landslide activity, as opposed to the real activity, was produced. An error matrix was used to construct various types of accuracy statistics, including overall accuracy (OA), kappa coefficient (κ), producer's accuracy (PA), and user's accuracy (UA) (Congalton, 1991). OA represents the percentage of correctly classified samples. κ is a widely used and powerful multivariate accuracy assessment technique. It measures of the overall statistical agreement of a confusion matrix. Therefore, it assesses the classification accuracy more rigorously (Thapa and Murayama, 2009). PA represents the amount of inaccuracy that occurs due to an omission (omission error) and demonstrates the likelihood of an actual class being correctly categorized, whereas UA is a measure of commission error, indicating the probability that a segment classified as predicted data actually represents the specific activity. The following equation shows the full formula set used in the accuracy assessment process:

$$OA = \frac{\sum_{i=1}^{n} m_{ii}}{\sum_{j=1}^{n}\sum_{i=1}^{n} m_{ij}} \tag{8}$$

$$\kappa = \frac{N\sum_{i=1}^{n} m_{ij}\ \sum_{i=1}^{n}(m_i + m + i)}{N^2 - \sum_{i=1}^{n}(m_i + m + i)} \tag{9}$$

$$PA = \frac{m_{ii}}{m_{+i}} \tag{10}$$

$$UA = \frac{m_{ii}}{m_{i+}} \tag{11}$$

where m_{i+} and m_{+I} represent the sum of the rows and columns of the confusion matrix and N is the sum of all the items in the confusion matrix.

Results and Discussion

Landslide Activity Classification

Machine learning methods (i.e. SVM and ANN) were adopted as the means of classifying landslide state of activity in the study area. These methods were used to classify the landslide state of activity of the delineated landslide polygon based on the VAIs input (Figure 2) in the training dataset, along with the landslide state of activity.

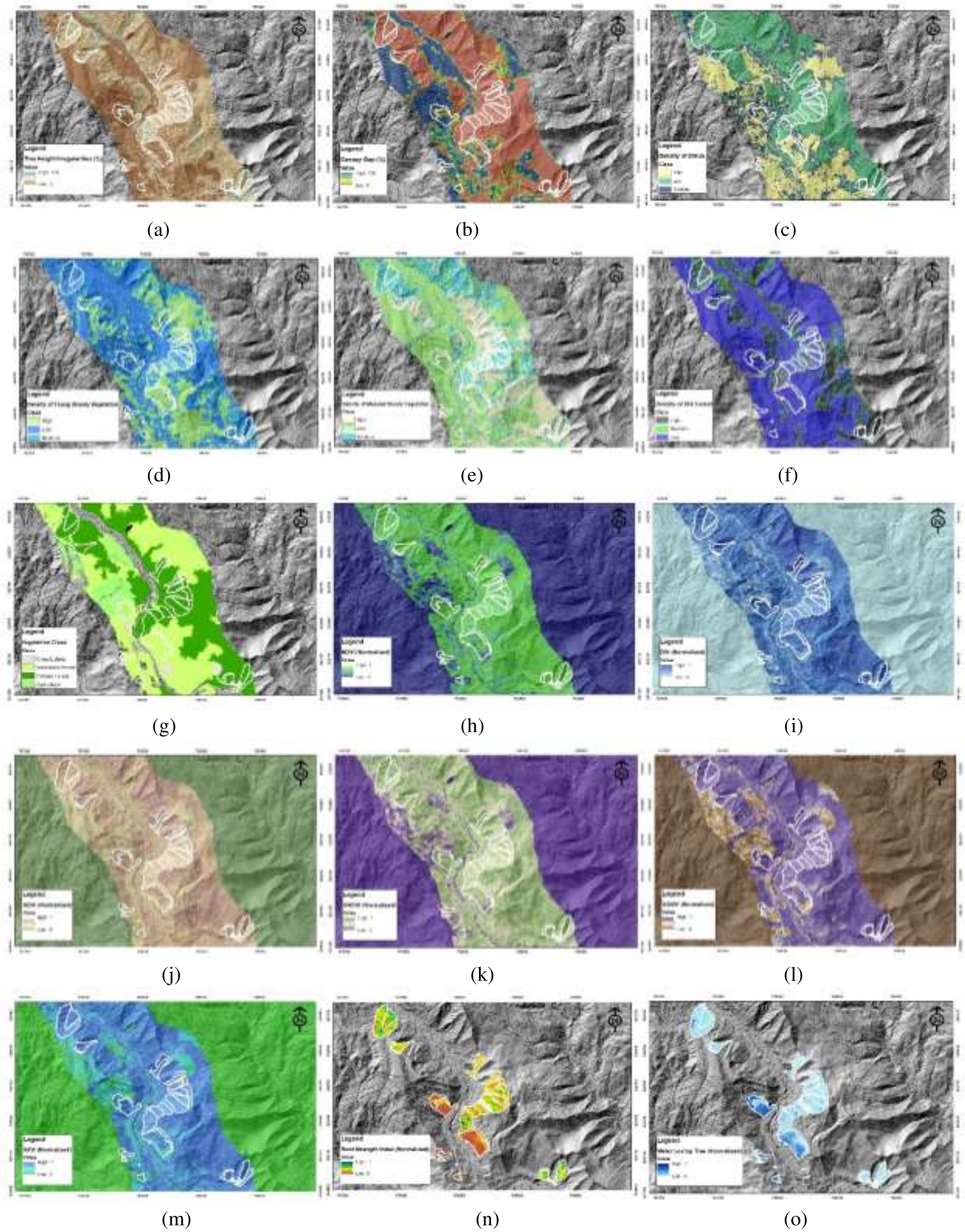

Figure 2. Map of (a) tree height irregularities, (b) canopy gap, (c) density of shrub, (d) density of young woody vegetation, (e) density of matured woody vegetation, (f) density of old forest, (g) vegetation classes, (h) NDVI, (i) DVI, (j) GDVI, (k) GNDVI, (l) OSAVI, (m) SAVI, (n) RSI, and (o) water loving trees

Support Vector Machine (SVM)

This section presents the classification results obtained with the SVM classification method where the manipulation was made based on different parameter setting. All results were obtained by varying the input parameters including kernel function, regularization parameter or cost (C), gamma (γ), and degree of polynomial (d) which only for polynomial kernel function. Two types of optimization method i.e. Grid Search (GS) and Genetic Algorithm (GA) were used in finding the best input parameter for landslide activity classification.

The performance of activity classification for deep-seated rotational landslides are presented in Figure 3. the classification using all the methods achieved moderate accuracy results with the OA between 48.2% and 68.6%, and κ is between 0.220 and 0.527. SVM with RBF kernel and GS (SVMR-GS) consistently reported the highest OA for all spatial resolution categories with 68.6%, 67.8%, 62.1%, 59.0%, and 54.9% for 0.5 m, 1 m, 5 m, 10 m, and 20 m resolution categories, respectively. Additionally, SVMR-GS produced higher κ values of 0.527 (0.5 m), 0.515 (1 m), 0.428 (5 m), 0.382 (10 m), and 0.318 (20 m). The increase of 13.7% of OA from 54.9% (20 m) to 68.6% (0.5 m) for SVMR-GS indicates that as the spatial resolution size decreases, the OA shows a good classification result. However, there were different scenarios for other methods except SVMR-GA, where the OA slightly increased under higher spatial resolution categories, i.e., SVML-GS (2.9%), SVMP-GS (3.3%), SVML-GA (4.8%), SVMP-GA (3.0%), and SVMR-GA (11.9%). Overall, the OA values of SVMR-GS and SVMR-GA reached more than 60% (resolution between 0.5 m and 5 m). This clearly demonstrates that the RBF kernel routinely achieves superior classification accuracy compared to any other kernel type.

In the case of shallow rotational landslide, The OA was recorded between 32.8% and 80.7%, and κ between 0.093 and 0.711. Again, SVMR-GS consistently reported the best OA for nearly all spatial resolution categories with 71.3%, 70.5%, 59.5%, 49.8%, and 65.8% for 0.5 m, 1 m, 5 m, 10 m, and 20 m resolution categories. Additionally, κ values of 0.708 (0.5 m), 0.706 (1 m), 0.610 (5 m), 0.566 (10 m), and 0.422 (20 m) indicate that SVMR-GS has a high classification accuracy. The OA for SVMR-GS increased from 60.7% (20 m) to 80.67% (0.5 m) at a rate of 19.9%, indicating that the OA remains steady when the spatial resolution size reduces. Other approaches, with the exception of SVML-GA and SVMR-GA, have different scenarios where the OA slightly increases as the spatial resolution increases, i.e. SVML-GS (4.3%), SVMP-GS (9.1%), SVML-GA (8.9%), SVMP-GA (33.7%), and SVMR-GA (38.1%). Among them, the OA values of SVMR-GS and SVMR-GA exceeded 80% (resolution of 0.5 m and 1 m). This clearly shows that the RBF kernel surpassed all other kernel types in terms of classification accuracy.

The analysis of the classification results for each activity classes is carried out by measuring the producer's accuracy (PA) and user's accuracy (UA). For deep-seated rotational landslides, the PA values ranged from 41.9%–60.8%, 53.1%–67.2%, and 43.4%–77.0% for active, dormant, and relict classes, respectively, while UA values ranged from 40.7%–68.8% (active), 46.7%–70.7% (dormant), and 50.0%–68.1% (relict), which can be categorized as moderate results. For the active class, it exhibited nearly the same PA and UA in the classified landslide, with the highest average values of 49.5% (PA) and 51.2% (UA). Dormant class results were substantially identical to active class results, with maximum averages of 58.8% and 55.1% for PA and UA, respectively, while the relict class recorded slightly higher values than the dormant class, with 58.1% (PA) and 63.3% (UA). For shallow rotational landslides, the assessment of PA and UA showed satisfactory accuracy results, especially for 0.5 m to 10 m spatial resolution categories. The PA values ranged from 64.3%–100.0%, 20.0%–75.6%, and 13.6%–86.8% for active, dormant, and relict classes, respectively, while UA values ranged from 24.0%–86.5% (active), 60.0%–81.8% (dormant), and 52.6%–87.5% (relict). By averaging the PA and UA values, SVM yielded moderate results with 78.6% (PA) and 79.7% (UA) for the active class, and 60.3% (PA) and 72.8% (UA) for the dormant class. Meanwhile, high PA and moderate UA values were recorded for the relict class. This indicates that high commissions of the relict class were observed in the classified results. By visualizing the classification results, as shown in Figure 4, the dormant class tends to be classified as a relict class (omission error), especially for large spatial resolution size categories. The misclassification of dormant as relict was obvious, especially for shallow rotational due to both classes' sharing similar vegetation characteristics. In summary, SVM successfully classify the landslide activity using VAIs whereas GS method produced higher accuracy results than GA approach. The results varied based on different kernel function. Kernel comparison clearly shows that RBF kernel outperformed other kernel type by consistently obtaining higher OA and κ values. This finding consistent with other studies (Kranjčić et al., 2019, Martins et al., 2016, Cho et al., 2017, Dabija et al., 2021). Analyzing the spatial resolution's effect on classification accuracy, better accuracy results were obtained for high spatial resolution categories regardless of the different parameter setting algorithm used.

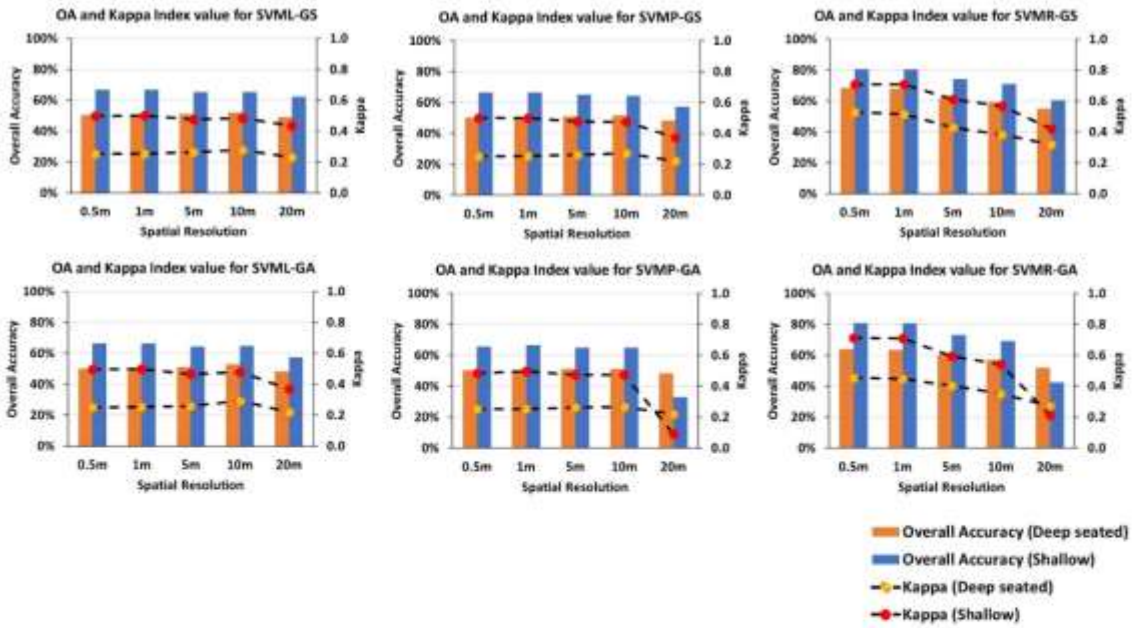

Figure 3. Overall accuracy and kappa coefficient of classified landslide activity for deep seated and shallow rotational landslides using SVM method

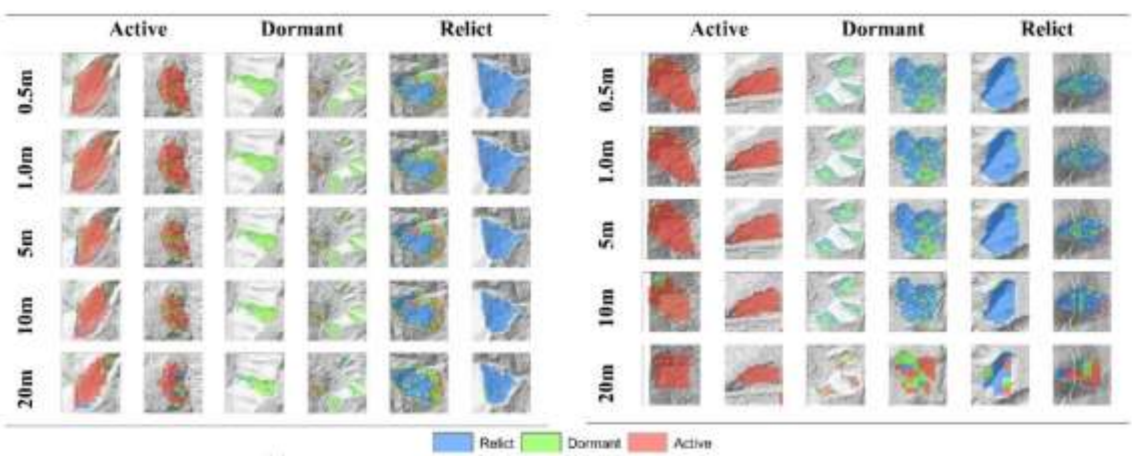

(a) (b)

Figure 4. Sample of classified landslide activity for (a) deep-seated, and (b) shallow rotational landslides with different spatial resolution categories using SVMR-GS method.

Artificial Neural Network (ANN)

The performance of activity classification for deep-seated and shallow rotational landslides are presented in Figure 5. For deep-seated rotational landslide, The OA was between 45.5% and 61.5%, and κ was between 0.181 and 0.420 for the *logistic* function. Meanwhile, the *tanh* function achieved 47.4%–58.7% and 0.201–0.377 for OA and κ, respectively. In general, ANN-MLP with *sag* (*logistic*) consistently reported the highest OA for almost all spatial resolution categories, with 61.4%, 61.5%, 60.5%, 56.3%, and 50.2% for 0.5 m, 1 m, 5 m, 10 m, and 20 m resolution categories, respectively. Additionally, *sag* (*logistic*) produced a higher κ value of 0.418 (0.5 m), 0.420 (1 m), 0.403 (5 m), 0.342 (10 m), and 0.246 (20 m). The increase of 11.3% of OA from 50.2% (20 m) to 61.5% (1 m) indicates that as the spatial resolution increases, the OA shows a good result. However, different scenarios apply for other methods because the OA increased slightly in higher spatial resolution categories. Overall, only *sag* (*logistic*) reached more than 60% (resolution of between 0.5 m and 5 m) of OA.

The classification accuracy was satisfactory for shallow rotational landslides. The OA was between 49.2% and 74.0%, and κ was between 0.253 and 0.610 for the *logistic* function. Meanwhile, *tanh* achieved 47.5%–74.7% and 0.215–0.620 for OA and κ, respectively. The combination of the *rprop*+ algorithm and the *tanh* activation function consistently reported the best OA almost for all spatial resolution categories with 74.1%, 74.7%, 73.3%, 68.1%, and 49.2% for 0.5 m, 1 m, 5 m, 10 m, and 20 m resolution categories, respectively. The OA for *rprop*+ (*tanh*) increased from 49.2% (20 m) to 74.7% (1 m) at a rate of 25.5%, indicating that the OA remains steady when the spatial resolution size reduces. Among them, all the approaches except *backprop* (*tanh*) and *slr* (*tanh*) exceeded 70% (resolution of 0.5 m, 1 m, and 5 m) of OA.

The analysis of the classification results for each activity classes is carried out by measuring the PA and UA. For deep-seated rotational landslides, the PA values ranged from 32.4%–55.3%, 45.8%–65.6%, and 44.6–69.3% for the active, dormant, and relict classes, respectively, while UA values ranged from 35.3%–60.5% (active), 48.1%–62.8% (dormant), and 41.6%–62.8% (relict), which can be categorised as moderate results. The average PA and UA values indicate that the active class recorded slightly higher UA than PA, with the highest average values of 52.9% and 48.4%, respectively. As shown in Figure 6, the combination of the dormant and relict classes can be observed in the active class. Meanwhile, the dormant and relict classes recorded identical results with the active class, where average PA values varied from 53.6% to 55.9% (dormant), and 52.0% to 61.7% (relict). In relation to shallow rotational landslides, all the combinations recorded reliable results. PA varied from 50.0% to 85.7%, 40.0% to 74.9%, and 36.4% to 75.7% for the active, dormant, and relict classes, respectively, whereas UA ranged from 33.3% to 82.3% (active), 44.0% to 73.7% (dormant), and 54.2% to 86.7%. (relict). In all combinations with distinct classes of spatial resolution, when comparing the average PA and UA values, the active class showed slightly greater UA than PA, with the highest recorded average values of 79.4% (UA) and 76.1% (PA). In contrast to the active class, the relict and dormant cases differed in that the PA values were slightly greater than UA values, particularly for higher spatial resolution categories. The highest average values for the dormant class were 70.6% (PA) and 69.4% (UA), and for the relict class, 70.1% (PA) and 69.4% (UA). In summary, ANN successfully classified the landslide state of activity using VAIs, whereas all the learning algorithms showed nearly equal OA values and were not significantly different among them. The type of activation function used also does not impact the quality of the results since the recorded OA values do not have much difference between them. Analyzing the spatial resolution's effect on classification accuracy, better accuracy results were obtained for high spatial resolution categories regardless of the different parameter setting algorithms used.

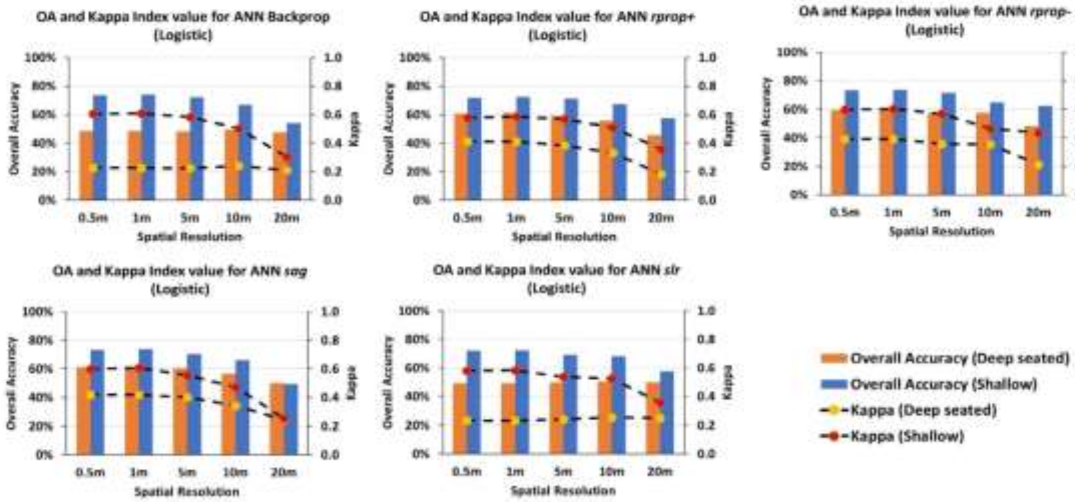

(a)

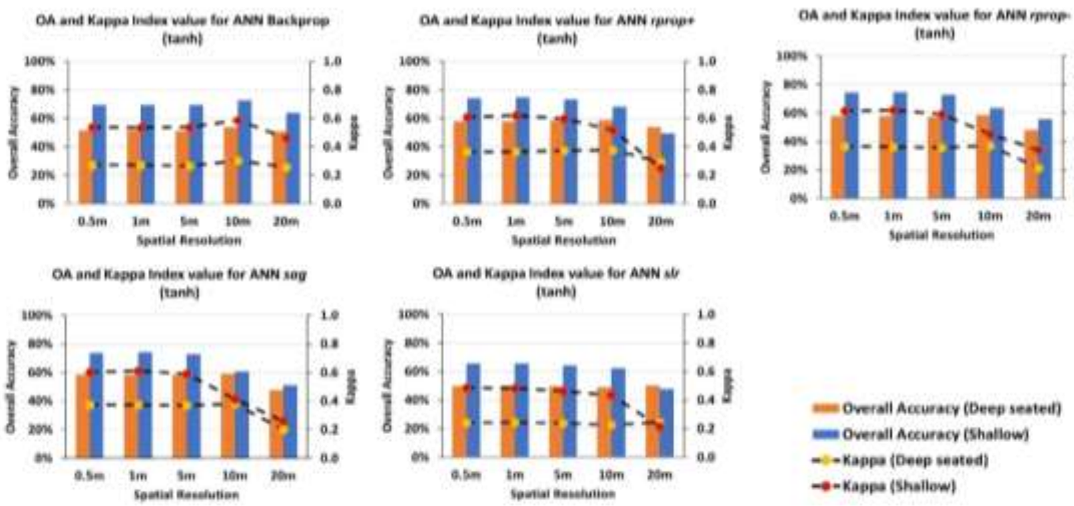

(b)

Figure 5. Overall accuracy and kappa coefficient of classified landslide activity using (a) sigmoid (*logistic*) and (b) hyperbolic tangent (*tanh*) activation functions

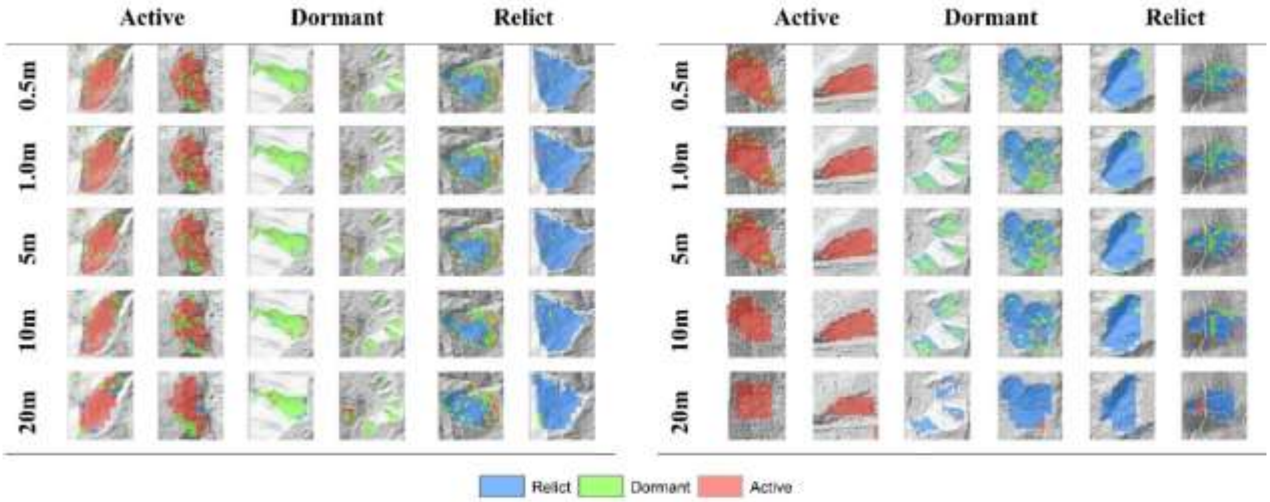

(a) (b)

Figure 6. Sample of classified landslide activity for (a) deep-seated rotational using ANN with *sag* (*logistic*) method, and (b) shallow rotational using ANN with *rprop+ tanh* method with different spatial resolution categories using ANN method.

Conclusion

In conclusion, this study introduces a novel approach to mapping the state of landslide activity in the Kundasang region of Sabah, Malaysia, by utilizing the Vegetation Anomalies Indicator (VAI) derived from high-resolution remotely sensed data. The methodology involves a combination of manual landslide inventory and VAI generation through high-resolution remote sensing data, which is then used to train machine learning models, namely Support Vector Machine (SVM) and Artificial Neural Network (ANN), using seven main VAIs. The findings of the study reveal that higher spatial resolution categories yield optimal results for both SVM and ANN methods. SVM outperforms ANN in classifying both deep-seated and shallow rotational landslides, achieving an overall accuracy of 68.6% and 80.7% respectively. The evaluation of SVM indicates that the radial basis function (RBF) kernel produces the highest accuracies, while ANN performs best when utilizing a hyperbolic tangent (tanh) activation function. Overall, this research demonstrates the potential for more accurate mapping and monitoring of landslide activity by employing the VAI method in tectonically active regions. By improving the understanding of landslide dynamics and providing timely information, this approach can contribute to enhancing disaster risk reduction and management strategies in such areas. The study opens up new possibilities for leveraging high-resolution remote sensing data and machine learning techniques in landslide assessment and monitoring, thereby aiding in the mitigation of landslide-related hazards.

Authors' contributions

Mohd Radhie Mohd Salleh and Muhammad Zulkarnain Abdul Rahman led the design of the study. Mohd Radhie Mohd Salleh conducted data processing and analysis, and finalized the manuscript with input from the other authors. The manuscript was reviewed and approved by Zamri Ismail, Mohd Faisal Abdul Khanan, Kasturi Devi Kanniah, Azman Ariffin, Wan Hazli Wan Kadir, Tam Tze Huey, and Mohd Asraff Asmadi.

Funding

Fundamental Research Grant Scheme, R.J130000.7852.5F396 are acknowledged for the partial funding of this research work as a fulfillment to the requirement of the PhD for the first author.

Competing interests

The authors confirm that they have no competing interests with any individual or organization.

References

Abdi, E. (2018). Root tensile force and resistance of several tree and shrub species of Hyrcanian forest, Iran. *Croatian Journal of Forest Engineering: Journal for Theory and Application of Forestry Engineering, 39*(2), 255-270.

Abe, S. (2005). *Support vector machines for pattern classification* (Vol. 2): Springer.

Afeni, T. B., & Cawood, F. T. (2013). Slope monitoring using total station: what are the challenges and how should these be mitigated? *South African Journal of Geomatics, 2*(1), 41-53.

Antonini, G., Ardizzone, F., Cardinali, M., Galli, M., Guzzetti, F., & Reichenbach, P. (2002). Surface deposits and landslide inventory map of the area affected by the 1997 Umbria-Marche earthquakes. *Bollettino della Società geologica italiana, 121*(1), 843-853.

Artese, S., & Perrelli, M. (2018). Monitoring a landslide with high accuracy by total station: a DTM-based model to correct for the atmospheric effects. *Geosciences, 8*(2), 46. doi:https://doi.org/10.3390/geosciences8020046

Ayalew, L., & Yamagishi, H. (2005). The application of GIS-based logistic regression for landslide susceptibility mapping in the Kakuda-Yahiko Mountains, Central Japan. *Geomorphology, 65*(1-2), 15-31. doi:https://doi.org/10.1016/j.geomorph.2004.06.010

Azlan, N. N. N., Simon, N., Hussin, A., & Roslee, R. (2016). *Soil properties of crocker formation and its influence on slope instability along the Ranau-Tambunan highway, Sabah.* Paper presented at the AIP Conference Proceedings.

Behling, R., Roessner, S., Kaufmann, H., & Kleinschmit, B. (2014). Automated spatiotemporal landslide mapping over large areas using rapideye time series data. *Remote Sensing, 6*(9), 8026-8055. doi:https://doi.org/10.3390/rs6098026

Berardino, P., Fornaro, G., Lanari, R., & Sansosti, E. (2002). A new algorithm for surface deformation monitoring based on small baseline differential SAR interferograms. *IEEE Transactions on Geoscience and remote sensing, 40*(11), 2375-2383. doi:https://doi.org/10.1109/igarss.2002.1025900

Bianchini, S., Raspini, F., Ciampalini, A., Lagomarsino, D., Bianchi, M., Bellotti, F., & Casagli, N. (2017). Mapping landslide phenomena in landlocked developing countries by means of satellite remote sensing data: the case of Dilijan (Armenia) area. *Geomatics, natural hazards and risk, 8*(2), 225-241. doi:https://doi.org/10.1080/19475705.2016.1189459

Bibi, T., Razak, K. A., Rahman, A. A., & Latif, A. (2017). *Spatio Temporal Detection and Virtual Mapping of Landslide Using High-Resolution Airborne Laser Altimetry (LiDAR) in Densely Vegetated Areas of Tropics*. Paper presented at the International Archives of the Photogrammetry, Remote Sensing & Spatial Information Sciences.

Bozzano, F., Mazzanti, P., Perissin, D., Rocca, A., De Pari, P., & Discenza, M. E. (2017). Basin scale assessment of landslides geomorphological setting by advanced InSAR analysis. *Remote Sensing, 9*(3), 267. doi:https://doi.org/10.3390/rs9030267

Brabb, E. E. (1991). The world landslide problem. *Episodes Journal of International Geoscience, 14*(1), 52-61. doi:https://doi.org/10.18814/epiiugs/1991/v14i1/008

Brabb, E. E., & Pampeyan, E. H. (1972). *Preliminary map of landslide deposits in San Mateo County, California*. Retrieved from

Brardinoni, F., Slaymaker, O., & Hassan, M. A. (2003). Landslide inventory in a rugged forested watershed: a comparison between air-photo and field survey data. *Geomorphology, 54*(3-4), 179-196. doi:https://doi.org/10.1016/s0169-555x(02)00355-0

Brokaw, N. V. (1982). The definition of treefall gap and its effect on measures of forest dynamics. *Biotropica*, 158-160. doi:https://doi.org/10.2307/2387750

Campbell, M. J., Dennison, P. E., Hudak, A. T., Parham, L. M., & Butler, B. W. (2018). Quantifying understory vegetation density using small-footprint airborne lidar. *Remote sensing of environment, 215*, 330-342. doi:https://doi.org/10.1016/j.rse.2018.06.023

Capilleri, P. P., Motta, E., & Raciti, E. (2016). Experimental study on native plant root tensile strength for slope stabilization. *Procedia Engineering, 158*, 116-121. doi:https://doi.org/10.1016/j.proeng.2016.08.415

Cardinali, M., Antonini, G., Reichenbach, P., & Guzzetti, F. (2001). Photo-geological and landslide inventory map for the Upper Tiber River basin. *CNR, Gruppo Nazionale per la Difesa dalle Catastrofi Idrogeologiche, Publication*(2154).

Cardinali, M., Guzzetti, F., & Brabb, E. E. (1990). *Preliminary maps showing landslide deposits and related features in New Mexico* (2331-1258). Retrieved from

Castagnetti, C., Bertacchini, E., Corsini, A., & Capra, A. (2013). Multi-sensors integrated system for landslide monitoring: critical issues in system setup and data management. *European journal of remote sensing, 46*(1), 104-124. doi:https://doi.org/10.5721/eujrs20134607

Chatwin, S. C., & Howes, D. (1991). A Guide for Management of Landslide Prone Terrain in the Pacific Northwest.

Chen, J.-W., Chue, Y.-S., & Chen, Y.-R. (2013). The application of the genetic adaptive neural network in landslide disaster assessment. *Journal of Marine Science and Technology, 21*(4), 442-452.

Cho, G.-S., Gantulga, N., & Choi, Y.-W. (2017). A comparative study on multi-class SVM & kernel function for land cover classification in a KOMPSAT-2 image. *KSCE Journal of Civil Engineering, 21*(5), 1894-1904. doi:https://doi.org/10.1007/s12205-016-1739-z

Cigna, F., Bianchini, S., & Casagli, N. (2013). How to assess landslide activity and intensity with Persistent Scatterer Interferometry (PSI): the PSI-based matrix approach. *Landslides, 10*(3), 267-283. doi:https://doi.org/10.1007/s10346-012-0335-7

Cigna, F., Ventisette, C. D., Liguori, V., & Casagli, N. (2011). Advanced radar-interpretation of InSAR time series for mapping and characterization of geological processes. *Natural Hazards and Earth System Sciences, 11*(3), 865-881. doi:https://doi.org/10.5194/nhess-11-865-2011

Congalton, R. G. (1991). A review of assessing the accuracy of classifications of remotely sensed data. *Remote sensing of environment, 37*(1), 35-46. doi:https://doi.org/10.1016/0034-4257(91)90048-b

Corsini, A., Castagnetti, C., Bertacchini, E., Rivola, R., Ronchetti, F., & Capra, A. (2013). Integrating airborne and multi-temporal long-range terrestrial laser scanning with total station measurements for mapping and monitoring a compound slow moving rock slide. *Earth Surface Processes and Landforms, 38*(11), 1330-1338. doi:https://doi.org/10.1002/esp.3445

Crawford, M. M. (2014). *Inventory mapping and characterization of landslides using LiDAR: Kenton and Campbell counties, Kentucky.* Paper presented at the Digital mapping techniques '11–12—workshop proceedings.

Cronk, J. K., & Fennessy, M. S. (2016). *Wetland plants: biology and ecology*: CRC press.

Dabija, A., Kluczek, M., Zagajewski, B., Raczko, E., Kycko, M., Al-Sulttani, A. H., . . . Corbera, J. (2021). Comparison of support vector machines and random forests for corine land cover mapping. *Remote Sensing, 13*(4), 777. doi:https://doi.org/10.3390/rs13040777

Duman, T. Y., Can, T., Emre, Ö., Keçer, M., Doğan, A., Ateş, Ş., & Durmaz, S. (2005). Landslide inventory of northwestern Anatolia, Turkey. *Engineering geology, 77*(1-2), 99-114. doi:https://doi.org/10.1016/j.enggeo.2004.08.005

Gaidzik, K., Ramírez-Herrera, M. T., Bunn, M., Leshchinsky, B. A., Olsen, M., & Regmi, N. R. (2017). Landslide manual and automated inventories, and susceptibility mapping using LIDAR in the forested mountains of Guerrero, Mexico. *Geomatics, natural hazards and risk, 8*(2), 1054-1079. doi:https://doi.org/10.1080/19475705.2017.1292560

Galli, M., Ardizzone, F., Cardinali, M., Guzzetti, F., & Reichenbach, P. (2008). Comparing landslide inventory maps. *Geomorphology, 94*(3-4), 268-289. doi:https://doi.org/10.1016/j.geomorph.2006.09.023

Ginzler, C., Bärtschi, H., Bedolla, A., Brassel, P., Hägeli, M., Hauser, M., . . . Uebersax, D. (2005). Manual for the Aerial Photo Interpretation within the Swiss Forest Inventory.

Golovko, D., Roessner, S., Behling, R., Wetzel, H.-U., & Kleinschmidt, B. (2015). Development of multi-temporal landslide inventory information system for southern Kyrgyzstan using GIS and satellite remote sensing. *Photogrammetrie-Fernerkundung-Geoinformation (PFG), 2015*(2), 157-172. doi:https://doi.org/10.1127/pfg/2015/0261

Gove, R., & Faytong, J. (2012). Machine learning and event-based software testing: classifiers for identifying infeasible GUI event sequences.

In *Advances in Computers* (Vol. 86, pp. 109-135): Elsevier.

Guzzetti, F., Cardinali, M., & Reichenbach, P. (1996). The Influence of Structural Setting and Lithology on Landslide Type and Pattern. *Environmental and Engineering Geoscience, II*(4), 531-555 %@ 1078-7275. doi:https://doi.org/10.2113/gseegeosci.ii.4.531

Guzzetti, F., Carrara, A., Cardinali, M., & Reichenbach, P. (1999). Landslide hazard evaluation: a review of current techniques and their application in a multi-scale study, Central Italy. *Geomorphology, 31*(1-4), 181-216. doi:https://doi.org/10.1016/s0169-555x(99)00078-1

Guzzetti, F., Mondini, A. C., Cardinali, M., Fiorucci, F., Santangelo, M., & Chang, K.-T. (2012). Landslide inventory maps: New tools for an old problem. *Earth-Science Reviews, 112*(1-2), 42-66. doi:https://doi.org/10.1016/j.earscirev.2012.02.001

Haneberg, W. C., Cole, W. F., & Kasali, G. (2009). High-resolution lidar-based landslide hazard mapping and modeling, UCSF Parnassus Campus, San Francisco, USA. *Bulletin of Engineering Geology and the Environment, 68*(2), 263-276. doi:https://doi.org/10.1007/s10064-009-0204-3

Harker, R. I. (1996). Curved tree trunks: indicators of soil creep and other phenomena. *The Journal of Geology, 104*(3), 351-358. doi:https://doi.org/10.1086/629830

Haugerud, R. A., Harding, D. J., Johnson, S. Y., Harless, J. L., Weaver, C. S., & Sherrod, B. L. (2003). High-resolution lidar topography of the Puget Lowland, Washington. *GSA Today, 13*(6), 4-10. doi:https://doi.org/10.1130/1052-5173(2003)13%3C0004:hltotp%3E2.0.co;2

Haykin, S. (2004). Neural Networks – A Comprehensive Foundation. *2*(2004), 41. doi:https://doi.org/10.1016/0925-2312(95)90026-8

Hede, A. N. H., Kashiwaya, K., Koike, K., & Sakurai, S. (2015). A new vegetation index for detecting vegetation anomalies due to mineral deposits with application to a tropical forest area. *Remote sensing of environment, 171*, 83-97. doi:https://doi.org/10.1016/j.rse.2015.10.006

Hooper, A., Segall, P., & Zebker, H. (2007). Persistent scatterer interferometric synthetic aperture radar for crustal deformation analysis, with application to Volcán Alcedo, Galápagos. *Journal of Geophysical Research: Solid Earth, 112*(B7). doi:https://doi.org/10.1029/2006jb004763

Hung, L. Q., Van, N. T. H., Son, P. V., Ninh, N. H., Tam, N., & Huyen, N. T. (2017). *Landslide Inventory Mapping in the Fourteen Northern Provinces of Vietnam: Achievements and Difficulties*, Cham %@ 978-3-319-59469-9.

Ian H. Witten, E. F., Mark A. Hall, Christopher Pal. (2017). Extending instance-based and linear models. In E. F. Ian H. Witten, Mark A. Hall, Christopher Pal (Ed.), *Data Mining (Fourth Edition)* (pp. 243–284): Morgan Kaufmann.

Ismail, Z., Rahman, M. Z. A., Salleh, M. R. M., & Yusof, A. R. M. (2015). Accuracy assessment of LIDAR-derived elevation value over vegetated terrain in tropical region. *Jurnal Teknologi, 73*(5). doi:https://doi.org/10.11113/jt.v73.4335

Iwahashi, J., Okatani, T., Nakano, T., Koarai, M., & Otoi, K. (2014). Landslide Susceptibility Analysis by Terrain and Vegetation Attributes Derived from Pre-event LiDAR data: a case study of granitic mountain slopes in Hofu, Japan. *INTERPRAEVENT2014 Pacific Rim, 20*.

Jaboyedoff, M., Oppikofer, T., Abellán, A., Derron, M.-H., Loye, A., Metzger, R., & Pedrazzini, A. (2012). Use of LIDAR in landslide investigations: a review. *Natural hazards, 61*(1), 5-28. doi:https://doi.org/10.1007/s11069-010-9634-2

Jackson Jr, L., Bobrowsky, P., & Bichler, A. (2012). Identification, maps and mapping—Canadian technical guidelines and best practices related to landslides: a national initiative for loss reduction. *Geological survey of Canada, Open file, 7059*. doi:https://doi.org/10.4095/292122

Jacobson, G. (1970). *Gunung Kinabalu area, East Malaysia*. Retrieved from

Johnson, A., Swanston, D., & McGee, K. (2000). Landslide Initiation, Runout, and Deposition Within Clearcuts and Old-Growth Forests of Alaska. *JAWRA Journal of the American Water Resources Association, 36*(1), 17-30. doi:https://doi.org/10.1111/j.1752-1688.2000.tb04245.x

Joyce, K. E., Samsonov, S., Levick, S. R., Engelbrecht, J., & Belliss, S. (2014). Mapping and monitoring geological hazards using optical, LiDAR, and synthetic aperture RADAR image data. *Natural hazards, 73*(2), 137-163. doi:https://doi.org/10.1007/s11069-014-1122-7

Kalia, A. C. (2018). Classification of landslide activity on a regional scale using persistent scatterer interferometry at the moselle valley (Germany). *Remote Sensing, 10*(12), 1880. doi:https://doi.org/10.1007/s11069-014-1122-7

Kavzoglu, T., Sahin, E. K., & Colkesen, I. (2014). Landslide susceptibility mapping using GIS-based multi-criteria decision analysis, support vector machines, and logistic regression. *Landslides, 11*(3), 425-439. doi:https://doi.org/10.1007/s10346-013-0391-7

Korup, O. (2005). Geomorphic imprint of landslides on alpine river systems, southwest New Zealand. *Earth Surface Processes and Landforms, 30*(7), 783-800. doi:https://doi.org/10.1002/esp.1171

Kotu, V., & Deshpande, B. (2014). *Predictive analytics and data mining: concepts and practice with rapidminer*: Morgan Kaufmann.

Kranjčić, N., Medak, D., Župan, R., & Rezo, M. (2019). Support vector machine accuracy assessment for extracting green urban areas in towns. *Remote Sensing, 11*(6), 655. doi:https://doi.org/10.3390/rs11060655

Li, Z., Shi, W., Lu, P., Yan, L., Wang, Q., & Miao, Z. (2016). Landslide mapping from aerial photographs using change detection-based Markov random field. *Remote sensing of environment, 187*, 76-90. doi:https://doi.org/10.1016/j.rse.2016.10.008

Luo, H., Wang, L., Wu, C., & Zhang, L. (2018). An improved method for impervious surface mapping incorporating LiDAR data and high-resolution imagery at different acquisition times. *Remote Sensing, 10*(9), 1349. doi:https://doi.org/10.3390/rs10091349

Łuszczyńska, K., Wistuba, M., & Malik, I. (2017). Dendrochronology as a source of data for landslide activity maps–an example from Beskid Żywiecki Mountains (Western Carpathians, Poland). *Environmental & Socio-economic Studies, 5*(3), 40-46. doi:https://doi.org/10.1515/environ-2017-0015

Marchesini, I., Santangelo, M., Fiorucci, F., Cardinali, M., Rossi, M., & Guzzetti, F. (2013). A GIS method for obtaining geologic bedding attitude. In *Landslide science and practice* (pp. 243-247): Springer.

Martins, S., Bernardo, N., Ogashawara, I., & Alcantara, E. (2016). Support vector machine algorithm optimal parameterization for change detection mapping in Funil Hydroelectric Reservoir (Rio de Janeiro State, Brazil). *Modeling Earth Systems and Environment, 2*(3), 1-10. doi:https://doi.org/10.1007/s40808-016-0190-y

McKean, J., & Roering, J. (2004). Objective landslide detection and surface morphology mapping using high-resolution airborne laser altimetry. *Geomorphology, 57*(3-4), 331-351. doi:https://doi.org/10.1016/s0169-555x(03)00164-8

Mezaal, M. R., Pradhan, B., Sameen, M. I., Mohd Shafri, H. Z., & Yusoff, Z. M. (2017). Optimized neural architecture for automatic landslide detection from high-resolution airborne laser scanning data. *Applied Sciences, 7*(7), 730. doi:https://doi.org/10.3390/app7070730

Mezaal, M. R., Pradhan, B., Shafri, H. Z. M., & Yusoff, Z. M. (2017). Automatic landslide detection using Dempster–Shafer theory from LiDAR-derived data and orthophotos. *Geomatics, natural hazards and risk, 8*(2), 1935-1954. doi:https://doi.org/10.1080/19475705.2017.1401013

Mohd Salleh, M., Ismail, Z., Mohd Ariff, S., Abd Rahman, M. Z., Abdul Khanan, M., Asmadi, M. A., & Razak, K. A. (2019). Spatial Prediction Models for Landslide Activity Mapping Using Vegetation Anomalies. *International Archives of the Photogrammetry, Remote Sensing & Spatial Information Sciences*. doi:https://doi.org/10.5194/isprs-archives-xlii-4-w16-441-2019

Moos, C. (2014). *How does forest structure affect landslide susceptibility? Statistical prediction models for shallow landslides integrating forest structure.* Master Thesis. ETH Zurich,

Moosavi, V., Talebi, A., & Shirmohammadi, B. (2014). Producing a landslide inventory map using pixel-based and object-oriented approaches optimized by Taguchi method. *Geomorphology, 204*, 646-656. doi:https://doi.org/10.1016/j.geomorph.2013.09.012

Muscolo, A., Bagnato, S., Sidari, M., & Mercurio, R. (2014). A review of the roles of forest canopy gaps. *Journal of Forestry Research, 25*(4), 725-736.

Musinguzi, M., & Asiimwe, I. (2014). Application of geospatial tools for landslide hazard assessment for Uganda. *South African Journal of Geomatics, 3*(3), 302-314. doi:https://doi.org/10.4314/sajg.v3i3.4

Otukei, J. R., & Blaschke, T. (2010). Land cover change assessment using decision trees, support vector machines and maximum likelihood classification algorithms. *International Journal of Applied Earth Observation and Geoinformation, 12*, S27-S31. doi:https://doi.org/10.1016/j.jag.2009.11.002

Pawłuszek, K., Borkowski, A., & Tarolli, P. (2017). *Towards The Optimal Pixel Size of Dem for Automatic Mapping of Landslide Areas*. Paper presented at the International Archives of the Photogrammetry, Remote Sensing & Spatial Information Sciences.

Perera, E., Gunaratne, A., & Samarasinghe, S. (2022). Participatory Landslide Inventory (PLI): An Online Tool for the Development of a Landslide Inventory. *Complexity, 2022*. doi:https://doi.org/10.1155/2022/2659203

Pirasteh, S., & Li, J. (2016). Landslides investigations from geoinformatics perspective: quality, challenges, and recommendations. *Geomatics, natural hazards and risk, 8*(2), 448-465. doi:https://doi.org/10.1080/19475705.2016.1238850

Pradhan, B. (2013). A comparative study on the predictive ability of the decision tree, support vector machine and neuro-fuzzy models in landslide susceptibility mapping using GIS. *Computers & Geosciences, 51*, 350-365. doi:https://doi.org/10.1016/j.cageo.2012.08.023

Pradhan, B., Jebur, M. N., Shafri, H. Z. M., & Tehrany, M. S. (2015). Data fusion technique using wavelet transform and Taguchi methods for automatic landslide detection from airborne laser scanning data and quickbird satellite imagery. *IEEE Transactions on Geoscience and remote sensing, 54*(3), 1610-1622. doi:https://doi.org/10.1109/tgrs.2015.2484325

Rahman, M., & Gorte, B. (2009). *Tree crown delineation from high resolution airborne lidar based on densities of high points.* Paper presented at the Proceedings ISPRS Workshop Laserscanning 2009, September 1-2, France, IAPRS, XXXVIII (3/W8), 2009.

Razak, K. A. (2014). *Airborne laser scanning for forested landslides investigation in temperate and tropical environments.* (Doctor of Philosophy). University of Twente, Netherlands.

Razak, K. A., Bucksch, A., Damen, M., van Westen, C., Straatsma, M., & de Jong, S. (2013). Characterizing tree growth anomaly induced by landslides using LiDAR. In *Landslide science and practice* (pp. 235-241): Springer.

Razavian, R. S., Greenberg, S., & McPhee, J. (2019). Biomechanics imaging and analysis. *Encyclopedia of Biomedical Engineering*, 488-500.

Roslee, R., Pirah, J. A., Madr, A. N., & Zikiri, M. F. (2020). Applicability Of The Geological Strength Index (GSI) Classification For The Trusmadi Formation At Sabah, Malaysia. *Earth Sciences Malaysia (ESMY), 4*(1), 77-81. doi:https://doi.org/10.26480/esmy.01.2020.77.81

Roslee, R., Zawawi, N. S. A., Tahir, S., & Omang, S. (2008). *Engineering geological assessment of slope failure in the Ranau to Tambunan area, Sabah, Malaysia.* Paper presented at the International Conference on Geotechnical & Highway Engineering: GEOTROPIKA 2008.

Rupšys, P. (2016). New insights into tree height distribution based on mixed effects univariate diffusion processes. *PloS one, 11*(12), e0168507. doi:https://doi.org/10.1371/journal.pone.0168507

Salleh, M. R. M., Ishak, N. I., Razak, K. A., Abd Rahman, M. Z., Asmadi, M. A., Ismail, Z., & Khanan, M. F. A. (2018). Geospatial Approach for Landslide Activity Assessment and Mapping Based on Vegetation Anomalies. *International Archives of the Photogrammetry, Remote Sensing and Spatial Information Sciences, 42*(4/W9). doi:https://doi.org/10.5194/isprs-archives-xlii-4-w9-201-2018

Samodra, G., Bhandary, N. P., & Yatabe, R. (2017). Landslide inventory: challenge for landslide hazard assessment in Indonesia. In *GIS Landslide* (pp. 135-159): Springer.

Samodra, G., Chen, G., Sartohadi, J., & Kasama, K. (2018). Generating landslide inventory by participatory mapping: an example in Purwosari Area, Yogyakarta, Java. *Geomorphology, 306*, 306-313. doi:https://doi.org/10.1016/j.geomorph.2015.07.035

Santangelo, á., Cardinali, á., Rossi, á., Mondini, A., & Guzzetti, F. (2010). Remote landslide mapping using a laser rangefinder binocular and GPS. *Natural Hazards and Earth System Sciences, 10*(12), 2539-2546. doi:https://doi.org/10.5194/nhess-10-2539-2010

Santangelo, M., Marchesini, I., Bucci, F., Cardinali, M., Fiorucci, F., & Guzzetti, F. (2015). An approach to reduce mapping errors in the production of landslide inventory maps. *Natural Hazards and Earth System Sciences, 15*(9), 2111-2126. doi:https://doi.org/10.5194/nhess-15-2111-2015

Satriano, V., Ciancia, E., Filizzola, C., Genzano, N., Lacava, T., & Tramutoli, V. (2023). Landslides Detection and Mapping with an Advanced Multi-Temporal Satellite Optical Technique. *Remote Sensing, 15*(3), 683. doi:https://doi.org/10.3390/rs15030683

Scaioni, M., Longoni, L., Melillo, V., & Papini, M. (2014). Remote sensing for landslide investigations: an overview of recent achievements and perspectives. *Remote Sensing, 6*(10), 9600-9652. doi:https://doi.org/10.3390/rs6109600

Schmidt, K., Roering, J., Stock, J., Dietrich, W., Montgomery, D., & Schaub, T. (2001). The variability of root cohesion as an influence on shallow landslide susceptibility in the Oregon Coast Range. *Canadian Geotechnical Journal, 38*(5), 995-1024. doi:https://doi.org/10.1139/t01-031

Shahabi, H., & Hashim, M. (2015). Landslide susceptibility mapping using GIS-based statistical models and Remote sensing data in tropical environment. *Scientific reports, 5*(1), 1-15. doi:https://doi.org/10.1038/srep09899

Silva, I., & Eugenio Naranjo, J. (2020). A systematic methodology to evaluate prediction models for driving style classification. *Sensors, 20*(6), 1692. doi:https://doi.org/10.3390/s20061692

Simeoni, L., Ferro, E., & Tombolato, S. (2015). Reliability of field measurements of displacements in two cases of viaduct-extremely slow landslide interactions. In *Engineering Geology for Society and Territory-Volume 2* (pp. 125-128): Springer.

Soeters, R., & Westen, C. J. (1996). *Slope instability recognition, analysis, and zonation.* Paper presented at the Landslides: investigation and mitigation.

Stefanini, M. C. (2004). Spatio-temporal analysis of a complex landslide in the Northern Apennines (Italy) by means of dendrochronology. *Geomorphology, 63*(3-4), 191-202. doi:https://doi.org/10.1016/j.geomorph.2004.04.003

Stiros, S. C., Vichas, C., & Skourtis, C. (2004). Landslide monitoring based on geodetically derived distance changes. *Journal of surveying engineering, 130*(4), 156-162. doi:https://doi.org/10.1061/(asce)0733-9453(2004)130:4(156)

Stokes, A. (2002). Biomechanics of tree root anchorage. *Plant roots: The hidden half*, 175-186. doi:https://doi.org/10.1201/9780203909423-19

Tating, F., Hack, H., & Jetten, V. (2013). *Weathering and detorioration as quantitative factors in slope design in humid tropical areas: case study Northern Kota Kinabalu, Sabah, Malaysia*. Engineering in Exotic Environments, (33, 1).

Tating, F. F. (2006). *Landslide Susceptibility Assessment Using Information Value Statistical Method: A Case Study On Northern Kota Kinabalu, Sabah.* Paper presented at the Proc. of International Symposium on Geotechnical Hazards: Prevention, Mitigation and Engineering Response, Yogyakarta, Indonesia.

Thapa, R. B., & Murayama, Y. (2009). Urban mapping, accuracy, & image classification: A comparison of multiple approaches in Tsukuba City, Japan. *Applied Geography, 29*(1), 135-144. doi:https://doi.org/10.1016/j.apgeog.2008.08.001

Tien Bui, D., Pradhan, B., Lofman, O., & Revhaug, I. (2012). Landslide susceptibility assessment in vietnam using support vector machines, decision tree, and Naive Bayes Models. *Mathematical problems in Engineering, 2012*. doi:https://doi.org/10.1155/2012/974638

Tien Bui, D., Shahabi, H., Shirzadi, A., Chapi, K., Alizadeh, M., Chen, W., . . . Hong, H. (2018). Landslide detection and susceptibility mapping by airsar data using support vector machine and index of entropy models in cameron highlands, malaysia. *Remote Sensing, 10*(10), 1527. doi:https://doi.org/10.3390/rs10101527

Tongkul, F. (1987). *Sedimentology and structure of the Crocker Formation in the Kota Kinabalu area, Sabah, east Malaysia.* Royal Holloway, University of London,

Tongkul, F. (2007). *Geological inputs in road design and construction in mountainous areas of West Sabah, Malaysia.* Paper presented at the

Proc. of the 2nd Malaysia-Japan Symposium on Geohazards and Geoenvironmental Engineering. City Bayview Hotel, Langkawi.

Tsai, Z.-X., You, G. J.-Y., Lee, H.-Y., & Chiu, Y.-J. (2012). Use of a total station to monitor post-failure sediment yields in landslide sites of the Shihmen reservoir watershed, Taiwan. *Geomorphology, 139*, 438-451. doi:https://doi.org/10.1016/j.geomorph.2011.11.008

Van Den Eeckhaut, M., Kerle, N., Hervás, J., & Supper, R. (2013). Mapping of landslides under dense vegetation cover using object-oriented analysis and LiDAR derivatives. In *Landslide science and practice* (pp. 103-109): Springer.

Van Den Eeckhaut, M., Poesen, J., Verstraeten, G., Vanacker, V., Nyssen, J., Moeyersons, J., . . . Vandekerckhove, L. (2007). Use of LIDAR-derived images for mapping old landslides under forest. *Earth Surface Processes and Landforms, 32*(5), 754-769. doi:https://doi.org/10.1002/esp.1417

Van Westen, C., & Getahun, F. L. (2003). Analyzing the evolution of the Tessina landslide using aerial photographs and digital elevation models. *Geomorphology, 54*(1-2), 77-89. doi:https://doi.org/10.1016/s0169-555x(03)00057-6

Van Westen, C. J., Van Asch, T. W. J., & Soeters, R. (2006). Landslide hazard and risk zonation—why is it still so difficult? *Bulletin of Engineering Geology and the Environment, 65*, 167–184. doi:https://doi.org/10.1007/s10064-005-0023-0

Vapnik, V. (2013). *The nature of statistical learning theory*: Springer science & business media.

Varnes, D. J. (1978). Slope movement types and processes. *Special report, 176*, 11-33.

Verma, N. K., Lamb, D. W., Reid, N., & Wilson, B. (2016). Comparison of canopy volume measurements of scattered eucalypt farm trees derived from high spatial resolution imagery and LiDAR. *Remote Sensing, 8*(5), 388. doi:https://doi.org/10.3390/rs8050388

Wang, D., Hollaus, M., Puttonen, E., & Pfeifer, N. (2016). Automatic and self-adaptive stem reconstruction in landslide-affected forests. *Remote Sensing, 8*(12), 974. doi:https://doi.org/10.3390/rs8120974

Wang, D., Hollaus, M., Schmaltz, E., Wieser, M., Reifeltshammer, D., & Pfeifer, N. (2016). Tree stem shapes derived from TLS data as an indicator for shallow landslides. *Procedia Earth and Planetary Science, 16*, 185-194. doi:https://doi.org/10.1016/j.proeps.2016.10.020

Watt, A. S. (1947). Pattern and process in the plant community. *Journal of ecology, 35*(1/2), 1-22. doi:https://doi.org/10.2307/2256497

Whitmore, T. (1982). On pattern and process in forests In: Newman EI, editor. The Plant Community as a Working Mechanism. In: Blackwell Scientific Publications, Oxford.

Wistuba, M., Malik, I., Gärtner, H., Kojs, P., & Owczarek, P. (2013). Application of eccentric growth of trees as a tool for landslide analyses: The example of Picea abies Karst. in the Carpathian and Sudeten Mountains (Central Europe). *Catena, 111*, 41-55. doi:https://doi.org/10.1016/j.catena.2013.06.027

Wu, C.-D., Cheng, C.-C., Chang, C.-C., Lin, C., Chang, K.-C., & Chuang, Y.-C. (2016). Gap shape classification using landscape indices and multivariate statistics. *Scientific reports, 6*(1), 1-10. doi:https://doi.org/10.1038/srep38217

Xun, Z., Zhao, C., Kang, Y., Liu, X., Liu, Y., & Du, C. (2022). Automatic extraction of potential landslides by integrating an optical remote sensing image with an InSAR-derived deformation map. *Remote Sensing, 14*(11), 2669. doi:https://doi.org/10.3390/rs14112669

Yang, W., Qi, W., Wang, M., Zhang, J., & Zhang, Y. (2017). Spatial and temporal analyses of post-seismic landslide changes near the epicentre of the Wenchuan earthquake. *Geomorphology, 276*, 8-15. doi:https://doi.org/10.1016/j.geomorph.2016.10.010

Yusoff, H. H. M., Razak, K. A., Yuen, F., Harun, A., Talib, J., Mohamad, Z., . . . Abd Razab, R. (2016). *Mapping of post-event earthquake induced landslides in Sg. Mesilou using LiDAR.* Paper presented at the IOP Conference Series: Earth and Environmental Science.

Zhang, L., Huang, R., Pei, X., & Li, S. (2016). Evolution analysis of a toppling landslide based on trees' growing—A case study of Erguxi Landslide, Lixian county, China. In *Landslides and Engineered Slopes. Experience, Theory and Practice* (pp. 2107-2112): CRC Press.

Zhong, C., Li, C., Gao, P., & Li, H. (2021). Discovering Vegetation Recovery and Landslide Activities in the Wenchuan Earthquake Area with Landsat Imagery.

Sensors, 21(15), 5243. doi:https://doi.org/10.3390/s21155243

Zirlewagen, D., & von Wilpert, K. (2001). Modeling water and ion fluxes in a highly structured, mixed-species stand. *Forest Ecology and Management, 143*(1-3), 27-37. doi:https://doi.org/10.1016/s0378-1127(00)00522-3